**International Journal of Applied Mathematics**

**Volume 33 No. 5 2020, 903-917**
ISSN: 1311-1728 (printed version); ISSN: 1314-8060 (on-line version)
**doi:** http://dx.doi.org/10.12732/ijam.v33i5.11

# IDENTIFICATION OF BURST PARAMETERS USING NUMERICAL QUASICONFORMAL MAPPING METHODS

Andrii Bomba[1], Mykhailo Boichura[2] §

[1]Dept. of Computer Sci. and Appl. Mathematics
[2] Research Department
[1,2] National University of Water and
Environmental Engineering
Rivne - 33028, UKRAINE

**Abstract:** The complex analysis methodology (method and corresponding algorithm) for solving the problems of applied quasipotential tomography developed by us, and which assumes (for each of the respective injections) the presence of only equipotential lines (with the given distributions of local velocities or values of stream functions) and streamlines (with known potential distributions on them) at the boundary of the domain is modified. This provides sufficient openness (for various additions, generalizations, etc.), flexibility (for mathematical manipulations) and greater accuracy (because, unlike common practical applications, sections of potential application are not considered "point-like") of the corresponding algorithm. A number of numerical experiments were performed in this work.

**AMS Subject Classification:** 30C62, 35J25, 65E05, 65N21
**Key Words:** applied quasipotential tomography; quasiconformal mapping; identification; nonlinear problems; numerical methods

## 1. Introduction

As a rule (see [1], [2], [3], [4], [5], [6], [8], [9], [12]), image reconstruction by

Received: July 20, 2020 

§Correspondence author

impedance tomography methods does not allow to obtain images of sufficient quality. This, in particular, is a consequence of the need to be limited to a finite number of injections in the calculations [8], [9], [12]. It is almost impossible to solve this problem. Also, one or another injection scheme [8], [9] or the method of image reconstruction [1], [8], [12] can give better or worse results depending on the structure of the object. The accuracy of the input data is proportional to the quality of measuring devices [8], [12]. Whereas there are almost no works on taking into account the current density distributions along the sections of electrode application to the test body (usually, the corresponding values are averaged). According to several comparisons with the results of the software product EIDORS [1], taking this data into account can significantly improve the quality of the obtained images [2]. To this aim, we described a methodology of image reconstruction, which assumes (for each of the respective injections) the presence of only equipotential lines (with the given distributions of local velocities or values of stream functions) and streamlines (with known potential distributions on them) at the boundary of the domain (see [2], [3], [5], [6]). This was done, in particular, with using the numerical quasiconformal mapping method, the advantages of which are described in [4]. Without reducing the generality, in further comparisons, we will use the results given in the article [3], where the reconstruction of the image is carried out in the presence of smooth local bursts of homogeneous materials. The corresponding conductivity coefficient (CC) is sought in the form:

$$\sigma(x, y, \chi, \alpha_1, ..., \alpha_s, \varepsilon_1, ..., \varepsilon_s, x_1, ..., x_s, y_1, ..., y_s) = \chi + \\ + \sum\nolimits_{k=1}^{s} \alpha_k / \left(1 + \left((x - x_k)^2 + (y - y_k)^2\right) / \varepsilon_k\right) \quad (1)$$

in [3], where $\chi$, $\alpha_k$, $\varepsilon_k$, $x_k$, $y_k$ $(k = 1, ..., s)$ are unknown parameters. Reconstruction of the image is carried out by alternating iterative application of the quasiconformal mapping method with fixed coordinates of boundary nodes and minimization the functional of sum of squared residuals between calculated CC distributions using the data from all injections.

A significant obstacle to asserting the prospects for further improvements of this approach is that it has been little applied in practice. And although there are certain successful comparisons with the results of the software product EIDORS [2], nevertheless, the corresponding methodology has not been sufficiently studied. To compare the methods, we consider the case of optimizing the sum of squared residuals between a priori known and iteratively calculated boundary values of quasipotential and stream functions [1], [5], [7], [8], [12], instead of the functional minimization options proposed in [2], [3].

This is the purpose of this work.

## 2. Numerical methods of complex analysis for solving the problem of applied quasipotential tomography

To date, attempts to minimize the corresponding functional precisely by numerical quasiconformal mapping methods have taken place in [5]. Similar to our previous works [2], [3], [6], it is assumed that quasiideal processes of particle motion (charges, fluids, etc.) take place in a single-connected curvilinear domain (plate, tomographic section, etc.) $G_z$ (Fig. 1(a)) bounded by a smooth closed curve $\partial G_z = \{(x,y) : x = \tilde{x}(\tau),\ y = \tilde{y}(\tau),\ 0 \le \tau \le 2\pi,\ \tilde{x}(0) = \tilde{x}(2\pi) = \tilde{x}_0,\ \tilde{y}(0) = \tilde{y}(2\pi) = \tilde{y}_0,$ *where* $\tilde{x}(\tau)$, $\tilde{y}(\tau)$ *are defined continuously differentiated functions*, $O(\tilde{x}_0, \tilde{y}_0)$ *is given an initial starting point*$\}$ due to the action of potential $\varphi_*^{(p)}$, $\varphi^{*(p)}$ differences ($\varphi^{*(p)} > \varphi_*^{(p)}$), which are given on selected equipotential lines $A_pB_p$, $C_pD_p$, where $A_p$, $B_p$, $C_p$, $D_p$ are marked points on $\partial G_z$; $p = 1, 2, ...$ is injection number (see, e.g. [5], [6]); $B_pC_p$ and $A_pD_p$ are impenetrable boundary streamlines. We model the injection of current through the tomographic cross-section, similarly to [2], [3], [5], [6] by sets of values $\{\tau_A^{(p)}, \tau_B^{(p)}, \tau_C^{(p)}, \tau_D^{(p)}\}$, according to which $A_p = \left(\tilde{x}(\tau_A^{(p)}), \tilde{y}(\tau_A^{(p)})\right)$, $B_p = \left(\tilde{x}(\tau_B^{(p)}), \tilde{y}(\tau_B^{(p)})\right)$, $C_p = \left(\tilde{x}(\tau_C^{(p)}), \tilde{y}(\tau_C^{(p)})\right)$, $D_p = \left(\tilde{x}(\tau_D^{(p)}), \tilde{y}(\tau_D^{(p)})\right)$. The boundary of the $G_z$ domain with the given four marked points corresponding to this injection is denoted by $\partial G_z^{(p)}$ ($z^{(p)} = x^{(p)} + iy^{(p)}$).

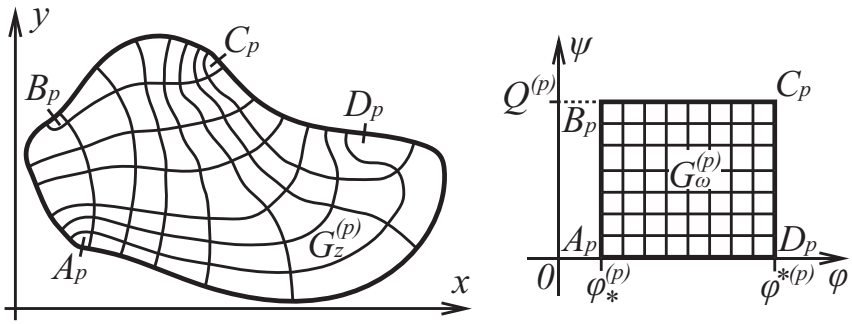


(a) (b)

Figure 1: Tomographic cross-section $G_z$ (a) and corresponding complex quasipotential domains $G_\omega^{(p)}$ (b)

Identification of CC $\sigma = \sigma(x, y)$ parameters (and concomitant finding $\varphi^{(p)} =$

$\varphi^{(p)}(x,y)$ functions with the known structure of the latter) in such an environment is traditionally carried out by solving equations of elliptic type [2], [3], [5], [6], [7], [8], [12]

$$div(\vec{j}^{(p)}) = 0 \tag{2}$$

under boundary conditions

$$\varphi|_{A_pB_p} = \varphi_*^{(p)},\ \varphi|_{C_pD_p} = \varphi^{*(p)}, \tag{3}$$

$$\varphi'^{(p)}_n\big|_{B_pC_p} = \varphi'^{(p)}_n\big|_{A_pD_p} = 0, \tag{4}$$

$$\varphi^{(p)}(M)\big|_{B_pC_p} = \bar{\varphi}^{(p)}(M), \varphi^{(p)}(M)\big|_{A_pD_p} = \underline{\varphi}^{(p)}(M), \tag{5}$$

$$\sigma\varphi'^{(p)}_n\big|_{A_pB_p} = \Psi_*^{(p)}(M), \sigma\varphi'^{(p)}_n\big|_{C_pD_p} = \Psi^{*(p)}(M), \tag{6}$$

where $M$ is a running point of the corresponding curve; $\vec{j}^{(p)} = \left(j_x^{(p)}(x,y), j_y^{(p)}(x,y)\right)$ is a current density (local velocity), which satisfies Ohm's (Darcy's) law $\vec{j}^{(p)} = \sigma\, grad\varphi^{(p)}$ [7], [8], [12]; $\varphi^{(p)} = \varphi^{(p)}(x,y)$ is quasipotential; $\vec{n}$ is an external normal to the corresponding section of the domain boundary. Functions $\bar{\varphi}^{(p)}(M) = \bar{\varphi}^{(p)}(\tau,...)$ $(\tau_C^{(p)} \le \tau \le \tau_B^{(p)})$, $\underline{\varphi}^{(p)}(M) = \underline{\varphi}^{(p)}(\tau,...)$ $(\tau_A^{(p)} \le \tau \le \tau_D^{(p)})$, $\Psi_*^{(p)}(M) = \Psi_*^{(p)}(\tau,...)$ $(\tau_B^{(p)} \le \tau \le \tau_A^{(p)})$, $\Psi^{*(p)}(M) = \Psi^{*(p)}(\tau,...)$ $(\tau_D^{(p)} \le \tau \le \tau_C^{(p)})$, as in [2], [3], [6], can be constructed by interpolating their experimentally obtained values $\bar{\varphi}^{(p)}_{\bar{i}^{(p)}}$, $\underline{\varphi}^{(p)}_{\underline{i}^{(p)}}$, $\Psi^{(p)}_{*j_*^{(p)}}$, $\Psi^{*(p)}_{j^{*(p)}}$ having some $\tau = \bar{\tau}^{(p)}_{\bar{i}^{(p)}}$, $\tau = \underline{\tau}^{(p)}_{\underline{i}^{(p)}}$, $\tau = \tau^{(p)}_{*j_*^{(p)}}$, $\tau = \tau^{*(p)}_{j^{*(p)}}$ at sections $B_pC_p$, $A_pD_p$, $A_pB_p$, $C_pD_p$, respectively $(\varphi_*^{(p)} \le \underline{\varphi}^{(p)}_{\underline{i}^{(p)}} \le \varphi^{*(p)}$, $\varphi_*^{(p)} \le \bar{\varphi}^{(p)}_{\bar{i}^{(p)}} \le \varphi^{*(p)}$, $\Psi^{(p)}_{*j_*^{(p)}} > 0$, $\Psi^{*(p)}_{j^{*(p)}} > 0$, $0 \le \bar{i}^{(p)} \le \bar{m}^{*(p)}+1, 0 \le \underline{i}^{(p)} \le \underline{m}_*^{(p)}+1, 0 \le j_*^{(p)} \le n_*^{(p)}+1, 0 \le j^{*(p)} \le n^{*(p)}+1)$.

We introduce $\psi^{(p)}(x,y)$ functions [4] (with, similarly, a known structure), which are complexly conjugated to $\varphi^{(p)}(x,y)$ and replace equations (2) and conditions (4) and (6) by

$$\sigma\varphi'^{(p)}_x = \psi'^{(p)}_y,\ \sigma\varphi'^{(p)}_y = -\psi'^{(p)}_x; \tag{7}$$

$$\psi^{(p)}\Big|_{A_pD_p} = 0,\ \psi^{(p)}\Big|_{B_pC_p} = Q^{(p)}; \tag{8}$$

$$\psi^{(p)}(M)\big|_{A_pB_p} = \psi_*^{(p)}(M), \psi^{(p)}(M)\big|_{C_pD_p} = \psi^{*(p)}(M), \tag{9}$$

where $\int_{MN} \sigma\frac{\partial\varphi^{(p)}}{\partial n}dl = Q^{(p)}$, $M \in B_pC_p$, $N \in A_pD_p$; $G_\omega^{(p)} = \{(\varphi,\psi) : \varphi_*^{(p)} \le \varphi \le \varphi^{*(p)}, 0 \le \psi \le Q^{(p)}\}$; $Q^{(p)}$ are discharges of a vector field (current) through

contact surfaces ($A_pB_p$ and $C_pD_p$); $\psi_*^{(p)}(M) = \int_{A_pM} \Psi_*^{(p)}(M)dl$, $\psi^{*(p)}(M) = \int_{D_pM} \Psi^{*(p)}(M)dl$; $dl$ is an arc element of the corresponding curve. Then we come to a series of more general boundary value problems on quasiconformal mappings $\omega = \omega^{(p)}(z) = \varphi^{(p)}(x,y) + i\psi^{(p)}(x,y)$ of physical domains $G_z^{(p)}$ (Fig. 1(a)) to the corresponding domains of complex quasipotential $G_\omega^{(p)}$ (Fig. 1(b)) under the condition of CC $\sigma = \sigma(x,y)$ identification [2], [3], [5], [6].

In [5] it is proposed to solve the problem (1), (3), (5), (7)-(9) under the condition of linearization of $\varphi^{(p)}(x,y)$ and $\psi^{(p)}(x,y)$ functions, their substitution into the functional (built from considerations of minimizing the calculated and a priori known quasipotential and stream functions at the boundary of the studied domain) of

$$\Phi = \sum_{p=1}^{\tilde{p}} \left( \sum_{N_1 \in A_pB_p} \left( \psi_*^{(p)}(N_1) - \psi^{(p)}(N_1) \right)^2 + \right.$$
$$+ \sum_{N_2 \in B_pC_p} \left( \bar{\varphi}^{(p)}(N_2) - \varphi^{(p)}(N_2) \right)^2 + \sum_{N_4 \in A_pD_p} \left( \underline{\varphi}^{(p)}(N_4) - \varphi^{(p)}(N_4) \right)^2 +$$
$$\left. + \sum_{N_3 \in C_pD_p} \left( \psi^{*(p)}(N_3) - \psi^{(p)}(N_3) \right)^2 \right) + \eta\, \Omega[\sigma] \to \min \quad (10)$$

type and its optimization with respect to the sought CC $\sigma = \sigma(x,y)$, where $N_1$, $N_2$, $N_3$ and $N_4$ are running points with a priori known $\psi_*^{(p)}(N_1)$, $\bar{\varphi}^{(p)}(N_2)$, $\psi^{*(p)}(N_3)$, $\underline{\varphi}^{(p)}(N_4)$ and calculated $\psi^{(p)}(N_1)$, $\varphi^{(p)}(N_2)$, $\psi^{(p)}(N_3)$, $\varphi^{(p)}(N_4)$ values of quasipotential and stream functions at the sections $A_pB_p$, $B_pC_p$, $C_pD_p$, $A_pD_p$, respectively; $\eta$ is a regularization parameter (which is solved according to the principle of generalized residues [13]); $\Omega[\sigma] = (\delta\sigma)^2$ is a stabilizing functional, $\delta$ is Kronecker symbol.

The corresponding problems in $x^{(p)} = x^{(p)}(\varphi,\psi)$, $y^{(p)} = y^{(p)}(\varphi,\psi)$ variables on quasiconformal mappings of complex quasipotential domains $G_\omega^{(p)}$ (Fig. 1(b)) on the corresponding physical domains $G_z^{(p)}$ (Fig. 1(a)) under the condition of identification of CC $\sigma = \sigma(x,y)$ [2], [3], [5], [6] consist in finding a solution of the system of generalizations of Laplace equations under boundary conditions and conditions of orthogonality at the boundary [4], and minimization of the functional (10).

The construction of a difference analogue of functional (10) in [5] is proposed to be carried out with respect to a finite so-called base set of points on the boundary. Based on the necessary condition for the existence of an extremum of

the function of many variables, a system of linear algebraic equations $A \cdot \vec{\sigma} = B$ with an unknown vector $\vec{\sigma} = (\sigma_1, \sigma_2, ..., \sigma_{n_*^{(p)}+\bar{m}^{(p)}+n^{*(p)}+\underline{m}^{(p)}})^T$ is obtained. Finally, the sought $\sigma = \sigma(x, y)$ function is approximated using interpolation in a predetermined set of boundary and internal (base) points.

## 3. Optimization of method

The disadvantages of the described approach are the following [12]: the need for interpolation of the CC and very frequent use of functions formed in this way, which, obviously, significantly slows down the speed of calculations; the linearization of quasipotential and stream functions, in combination with the finite number of injections and the "noise" in the input data, significantly "distorts" the result; the use of the matrix inversion procedure in an explicit form, because of which the computational process can be unstable if the initial CC approximation is unsuccessfully selected. Therefore (primarily due to particularly "strict" conditions of convergence), using the method [5] is problematic and corresponding comparisons with the approach described in [3] are only advisable in a very limited class of cases.

We propose an approach similar to [5] to solve the problem of image reconstruction based on minimization of the functional (10), but instead of linearizing the flow and quasipotential functions, we use the expression $\sigma \frac{\partial \varphi^{(p)}}{\partial l} = \frac{\partial \psi^{(p)}}{\partial s}$, that follows from Ohm's law and generalizations of the Cauchy-Riemann conditions, where $\partial l$ and $\partial s$ are elements of lengths along streamlines and equipotential lines, respectively. In this case

$$\begin{aligned} \psi^{(p)}(N_1) &= \psi^{(p)}(M_1) + \textstyle\int_{M_1N_1} \varphi_l'^{(p)} \sigma ds, \\ \varphi^{(p)}(N_2) &= \varphi^{(p)}(M_2) + \textstyle\int_{M_2N_2} \psi_s'^{(p)} / \sigma dl, \\ \psi^{(p)}(N_3) &= \psi^{(p)}(M_3) + \textstyle\int_{M_3N_3} \varphi_l'^{(p)} \sigma ds, \\ \varphi^{(p)}(N_4) &= \varphi^{(p)}(M_4) + \textstyle\int_{M_4N_4} \psi_s'^{(p)} / \sigma dl. \end{aligned} \tag{11}$$

Here $M_1$, $M_2$, $M_3$, $M_4$ and $N_1$, $N_2$, $N_3$, $N_4$ are the running points on the $A_pB_p$, $B_pC_p$, $C_pD_p$, $A_pD_p$ sections, respectively ($M_1 \in [A_p, N_1)$, $M_2 \in [B_p, N_2)$, $M_3 \in [D_p, N_3)$, $M_4 \in [A_p, N_4)$). We obtain the final form of the minimizing functional by substituting (11) into (10) for $\eta\,\Omega = \sum_{k=1}^{s}(\eta_k \alpha_k^2 + \eta_{s+k}\varepsilon_k^2)$ [6], where $\eta_k$ are regularization parameters. It should be noted that the adjustment (regularization), first of all, requires those components of the CC, which are relatively little affected by a priori (exact) data from the border. These are $\alpha_k$, $\varepsilon_k$, $x_k$, $y_k$ parameters. We assume that we do not have a priori information about

the coordinates of the bursts (because in the work [3], with which we compare the results, such information was not used). There are $\alpha_k$ and $\varepsilon_k$ parameters left. The latter especially need regularization, because the corresponding bursts become too flat when $\varepsilon_k$ values are very large and they in some way replace the $\chi$ parameter.

We present the corresponding difference analogues of problem (1), (3), (5), (7)-(10) taking into account (11) in the grid domains $G_\omega^{\gamma(p)} = \left\{(\varphi_i^{(p)}, \psi_j^{(p)}) : \varphi_i^{(p)} = \varphi_*^{(p)} + i\Delta\varphi^{(p)}, i=\overline{0,m^{(p)}+1}; \psi_j^{(p)} = j\Delta\psi^{(p)}, j=\overline{0,n^{(p)}+1}; \Delta\varphi^{(p)} = \frac{\varphi^{*(p)}-\varphi_*^{(p)}}{m^{(p)}+1}, \Delta\psi^{(p)} = \frac{Q^{(p)}}{n^{(p)}+1}, \gamma^{(p)}=\frac{\Delta\varphi^{(p)}}{\Delta\psi^{(p)}}, m^{(p)}, n^{(p)} \in N\right\}$ similarly to [2], [3], [4], [5], [6]. In particular, the systems of generalizations of Laplace equations and orthogonality conditions for boundary nodal points are approximated using a "cross-type" scheme, and left and right first-order difference schemes, respectively, where $\gamma^{(p)}$ are quasiconformal invariants [4] for the corresponding domains $G_\omega^{\gamma(p)}$.

It is expedient to construct the difference analogue of the functional (10) in such a way that a priori data at the boundary are taken into account as much as possible on the one hand, and quasiconformity errors do not accumulate on the other. The latter reach quite large values, especially in the vicinity of angular boundary points of streamlines and equipotential lines, which cause instability of the iterative process. For this purpose, applying the formula of the left rectangles to the integrals included in (10) for $M_1 = A_p$, $M_2 = B_p$, $M_3 = D_p$, $M_4 = A_p$ and performing elementary transformations, we obtain:

$$\Phi = \Phi_* + \bar{\Phi} + \Phi^* + \underline{\Phi} + \Omega \to \min, \tag{12}$$

where

$$\underline{\Phi} = \sum_{\substack{p,\underline{i}=1 \\ (\tau_{AD_{i-1}}^{(p,l)} < \underline{\tau_i}^{(p)} \le \tau_{AD_i}^{(p,l)})}}^{\tilde{p},\underline{m}^{(p)}+1} \left( \varphi_*^{(p)} - \underline{\varphi_i}^{(p)} + \left( \sum_{i_2=1}^{i-1} \frac{\sigma_{i_2-1,0}^{(l)}}{\sigma_{i_2-1,0}^{(l+1)}} + \right.\right.$$
$$\left.\left. + \frac{\sigma_{i-1,0}^{(l)}}{\sigma_{i-1,0}^{(l+1)}} \sqrt{\frac{(\underline{x_i}^{(p)} - x_{i-1,0}^{(p,l)})^2 + (\underline{y_i}^{(p)} - y_{i-1,0}^{(p,l)})^2}{(x_{i,0}^{(p,l)} - x_{i-1,0}^{(p,l)})^2 + (y_{i,0}^{(p,l)} - y_{i-1,0}^{(p,l)})^2}} \right) \Delta\varphi^{(p)} \right)^2,$$

$$\Phi_* = \sum_{\substack{p,j_*=1 \\ (\tau_{AB_{j-1}}^{(p,l)} < \tau_{*j_*}^{(p)} \le \tau_{AB_j}^{(p,l)})}}^{\tilde{p},n_*^{(p)}+1} \left( -\psi_{*j_*}^{(p)} + \left( \sum_{j_2=1}^{j-1} \frac{\sigma_{0,j_2-1}^{(l+1)}}{\sigma_{0,j_2-1}^{(l)}} + \right.\right.$$
$$\left.\left. + \frac{\sigma_{0,j-1}^{(l+1)}}{\sigma_{0,j-1}^{(l)}} \sqrt{\frac{(x_{*j_*}^{(p)} - x_{0,j-1}^{(p,l)})^2 + (y_{*j_*}^{(p)} - y_{0,j-1}^{(p,l)})^2}{(x_{0,j}^{(p,l)} - x_{0,j-1}^{(p,l)})^2 + (y_{0,j}^{(p,l)} - y_{0,j-1}^{(p,l)})^2}} \right) \Delta\psi^{(p,l)} \right)^2,$$

$$\bar{\Phi} = \sum_{\substack{p,\bar{i}=1 \\ (\tau_{BC_{i-1}}^{(p,l)} < \bar{\tau}_{\bar{i}}^{(p)} \le \tau_{BC_i}^{(p,l)})}}^{\tilde{p},\bar{m}^{(p)}+1} \left( \bar{\varphi}_{\bar{i}}^{(p)} - \varphi_*^{(p)} - \Delta\varphi^{(p)} \left( \sum_{i_2=1}^{i-1} \frac{\sigma_{i_2-1,n^{(p)}+1}^{(l)}}{\sigma_{i_2-1,n^{(p)}+1}^{(l+1)}} + \right. \right.$$

$$\left. \left. + \frac{\sigma_{i-1,n^{(p)}+1}^{(l)}}{\sigma_{i-1,n^{(p)}+1}^{(l+1)}} \sqrt{\frac{(\bar{x}_{\bar{i}}^{(p)} - x_{i-1,n^{(p)}+1}^{(p,l)})^2 + (\bar{y}_{\bar{i}}^{(p)} - y_{i-1,n^{(p)}+1}^{(p,l)})^2}{(x_{i,n^{(p)}+1}^{(p,l)} - x_{i-1,n^{(p)}+1}^{(p,l)})^2 + (y_{i,n^{(p)}+1}^{(p,l)} - y_{i-1,n^{(p)}+1}^{(p,l)})^2}} \right) \right)^2,$$

$$\Phi^* = \sum_{\substack{p,j^*=1 \\ (\tau_{CD_{j-1}}^{(p,l)} < \tau_{j^*}^{*(p)} \le \tau_{CD_j}^{(p,l)})}}^{\tilde{p},n^{*(p)}+1} \left( \psi_{j^*}^{*(p)} - \Delta\psi^{(p,l)} \left( \sum_{j_2=1}^{j-1} \frac{\sigma_{m^{(p)}+1,j_2-1}^{(l+1)}}{\sigma_{m^{(p)}+1,j_2-1}^{(l)}} + \right. \right.$$

$$\left. \left. + \frac{\sigma_{m^{(p)}+1,j-1}^{(l+1)}}{\sigma_{m^{(p)}+1,j-1}^{(l)}} \sqrt{\frac{(x_{j^*}^{*(p)} - x_{m^{(p)}+1,j-1}^{(p)})^2 + (y_{j^*}^{*(p)} - y_{m^{(p)}+1,j-1}^{(p)})^2}{(x_{m^{(p)}+1,j}^{(p)} - x_{m^{(p)}+1,j-1}^{(p)})^2 + (y_{m^{(p)}+1,j}^{(p)} - y_{m^{(p)}+1,j-1}^{(p)})^2}} \right) \right)^2;$$

$x_{i,j}^{(p)} = x^{(p)}(\varphi_i^{(p)}, \psi_j^{(p)})$, $y_{i,j}^{(p)} = y^{(p)}(\varphi_i^{(p)}, \psi_j^{(p)})$, $\sigma_{i,j}^{\gamma(p)} = \sigma\left(x_{i,j}^{(p)}, y_{i,j}^{(p)}\right)$, $(x_{i,j}^{(p)}, y_{i,j}^{(p)}) \in G_z^{\gamma(p)}$; $l = 0, 1, ...$ is an approximation number; $\underline{\tau}_{\underline{i}}^{(p)}$, $\tau_{*j_*}^{(p)}$, $\bar{\tau}_{\bar{i}}^{(p)}$, $\tau_{j^*}^{*(p)}$ ($\underline{i} = \overline{0, \underline{m}^{(p)}+1}$, $\bar{i} = \overline{0, \bar{m}^{(p)}+1}$, $j_* = \overline{0, n_*^{(p)}+1}$, $j^* = \overline{0, n^{*(p)}+1}$) are a priori known parameters of setting the $(\underline{x}_{\underline{i}}^{(p)}, \underline{x}_{\underline{i}}^{(p)})$, $(\bar{x}_{\bar{i}}^{(p)}, \bar{x}_{\bar{i}}^{(p)})$, $(x_{*j_*}^{(p)}, x_{*j_*}^{(p)})$, $(x_{j^*}^{*(p)}, x_{j^*}^{*(p)})$ points (by $x = \tilde{x}(\tau)$, $y = \tilde{y}(\tau)$) functions) on the $A_pD_p$, $B_pC_p$, $A_pB_p$, $C_pD_p$ sections with the corresponding values of the potential and stream functions $\underline{\varphi}_{\underline{i}}^{(p)}$, $\bar{\varphi}_{\bar{i}}^{(p)}$, $\psi_{*j_*}^{(p)}$, $\psi_{j^*}^{*(p)}$; $\underline{m}^{(p)}$, $\bar{m}^{(p)}$, $n_*^{(p)}$, $n^{*(p)}$ is the number of such points; $\tau_{AD_i}^{(p,l)}$, $\tau_{BC_i}^{(p,l)}$, $\tau_{AB_j}^{(p,l)}$, $\tau_{CD_j}^{(p,l)}$ ($i = \overline{0, m^{(p)}+1}$, $j = \overline{0, n^{(p)}+1}$) are the calculated parameters of setting the boundary nodes on the $A_pD_p$, $B_pC_p$, $A_pB_p$, $C_pD_p$ sections, respectively.

The **algorithm** for solving the initial problem consists of alternate parameterization of quasiconformal invariants, internal and boundary nodes of mesh domains $G_z^{\gamma(p)}$, CC with using the ideas of the block iteration method [4]. Namely: we set the number of injections $\tilde{p}$, the boundary of domains $G_z^{(p)}$ (by functions $x = \tilde{x}(\tau)$, $y = \tilde{y}(\tau)$), parameters $\tau_A^{(p)}$, $\tau_B^{(p)}$, $\tau_C^{(p)}$, $\tau_D^{(p)}$, quasipotentials $\varphi_*^{(p)}$, $\varphi^{*(p)}$, parameters $m^{(p)}$, $n^{(p)}$ of partitioning of domains $G_\omega^{\gamma(p)}$, the value of $\delta_1$, which is responsible for the accuracy of the algorithm. In this case, we calculate the coordinates of the angular points $A_p$, $B_p$, $C_p$, $D_p$ on $\partial G_z^{(p)}$ and $\Delta\varphi^{(p)} = \frac{\varphi^{*(p)} - \varphi_*^{(p)}}{m^{(p)}+1}$. Then set the values of local velocities $\Psi_{*j}^{(p)}$, $\Psi_j^{*(p)}$ (and, therefore, the stream functions $\psi_{*j}^{(p)}$, $\psi_j^{*(p)}$) and potentials $\bar{\varphi}_i^{(p)}$, $\underline{\varphi}_i^{(p)}$ for some arguments $\tau_{*j}^{(p)}$, $\tau_j^{*(p)}$, $\bar{\tau}_i^{(p)}$, $\underline{\tau}_i^{(p)}$ (results of physical measurements), respectively.

The initial approximations of the coordinates of the boundary $x_{0,j}^{(p,0)}$, $y_{0,j}^{(p,0)}$,

$x^{(p,0)}_{i,n^{(p)}+1}$, $y^{(p,0)}_{i,n^{(p)}+1}$, $x^{(p,0)}_{m^{(p)}+1,j}$, $y^{(p,0)}_{m^{(p)}+1,j}$, $x^{(p,0)}_{i,0}$, $y^{(p,0)}_{i,0}$ $(0 \le i \le m^{(p)}+1,\ 0 \le j \le n^{(p)}+1,\ p=\overline{1,\tilde{p}})$ and internal $x^{(p,0)}_{i,j}$, $y^{(p,0)}_{i,j}$ $(1 \le i \le m^{(p)},\ 1 \le j \le n^{(p)},\ p=\overline{1,\tilde{p}})$ nodes, and the parameters $\chi^{(0)}$, $\alpha^{(0)}_k$, $\varepsilon^{(0)}_k$, $x^{(0)}_k$, $y^{(0)}_k$ $(k=1,...,s)$ that determine the CC, are formed, for example, as in [2], [3], [4], [6]. In this case, we calculate the initial approximations of the values of quasiconformal invariants [4] and $\Delta\psi^{(p,0)} = \Delta\varphi^{(p)}/\gamma^{(p,0)}$.

The iterative process of reconstruction consists of the following stages: the coordinates of boundary and internal nodes, quasiconformal invariants and $\Delta\psi^{(p,r)} = \Delta\varphi^{(p)}/\gamma^{(p,r)}$ (here $r=0,1,...$ is the iteration step number) are specified sequentially [4]; this procedure is repeated until the conditions for completing the iterative process of constructing velocity fields are fulfilled, among which may be [2], [4] with the accuracy parameter $\delta_1$; functional (12) is minimized for the sought $\chi^{(l)}$, $\alpha^{(l)}_k$, $\varepsilon^{(l)}_k$, $x^{(l)}_k$, $y^{(l)}_k$ $(k=1,...,s)$ using one of the global optimization methods (see, e.g., [11]); it is checked whether the functional value (12) is less than $\delta_2$. In case of non-fulfillment of this condition, we start the iterative process anew, otherwise, we build the corresponding reconstructed image and, if necessary, electrodynamic meshes, complex quasipotential domains or calculate current density fields using the formula $\vec{j}^{(p)} = \sigma(x,y)\, grad\varphi^{(p)}$ etc. [3], [4].

## 4. The results of approximate calculations

Let us make a series of comparisons between the results of numerical experiments of image reconstruction obtained by the algorithm described above (for definiteness, we will call it algorithm $A$) and described in [3] (similarly we will call it algorithm $B$), using the simulated annealing method [11] to minimize functional (12), with the input data given in [3], in particular:

$$\tilde{x}(\tau) = 150\cos\tau, \tilde{y}(\tau) = 100\sin\tau,$$

$$\tau^{(p)}_A = \pi/8 + (p-1)\,\pi/\tilde{p} + \pi, \tau^{(p)}_B = \tau^{(p)}_A - \pi/4,$$

$$\tau^{(p)}_C = \tau^{(p)}_A - \pi, \tau^{(p)}_D = \tau^{(p)}_C - \pi/4, m^{(p)} = 100, \delta_1 = 25,$$

$$\varphi^{(p)}_* = 0, \varphi^{*(p)} = 1, \chi^{(0)} = \varepsilon^{(0)}_k = 1, \alpha^{(0)}_k = x^{(0)}_k = y^{(0)}_k = 0, \tag{13}$$

$$0.2 \le \chi \le 1.5, 0 \le \alpha_k \le 2, 10^{-2} \le \varepsilon_k \le 10^5,$$

$$-150 \le x_k \le 150, -100 \le y_k \le 100\ (k=1,...,s),$$

$$\eta_k = 0.01(k = \overline{1,s}), \eta_k = 0.000001\,(k = \overline{s+1,2s}).$$

Here, the choice of parameters $\tau_A^{(p)}$, $\tau_B^{(p)}$, $\tau_C^{(p)}$, $\tau_D^{(p)}$ was carried out similarly to the polar scheme of quasipotential application [9], which is most effective when inhomogeneities are placed at some distance from the boundary of the domain and its center; the corresponding $s$, $\chi$, $\alpha_k$, $\varepsilon_k$, $x_k$, $y_k$ $(k = 1, ..., s)$ are selected by the same logic (see Table 1(a),

| | $p$ | $\chi$ | $\alpha_1$ | $\varepsilon_1$ | $x_1$ | $y_1$ |
|---|---|---|---|---|---|---|
| a) | – | 0.5 | 1 | 200 | –95 | –12 |
| b) | 1,2,3,. . . ,40 | 0.5039 | 1.3029 | 128.625 | –102.187 | –13.0209 |
| c) | 1,2,3,. . . ,40 | 0.4727 | 1.1719 | 278.497 | –80.718 | –8.7694 |
| d) | 1,2,3,. . . ,20 | 0.4744 | 1.1712 | 274.7286 | –80.7618 | –8.4726 |
| e) | 1,2,3,. . . ,20 | 0.4999 | 1.2796 | 126.1498 | –106.09 | –14.619 |
| f) | 1,9,17,25,33 | 0.5127 | 1.2663 | 124.846 | –109.013 | –19.6638 |
| g) | 1,9,17,25,33 | 0.4722 | 1.198 | 267.8533 | –81.2635 | –8.7357 |
| h) | 1 | 0.944 | 2 | 202.784 | –101.66 | –72.812 |
| i) | 1 | 0.4857 | 0.4495 | 993.0104 | –82.576 | –17.6735 |
| j) | 20 | 0.5307 | 2 | 235.9537 | –100.033 | –72.1579 |
| k) | 20 | 0.4421 | 1.9348 | 278.815 | –74.9674 | –7.5969 |

Table 1: CC distributions for examples with one local burst, where (a) is an etalon, (b, d, f, h, j) and (c, e, g, i, k) are calculated according to the algorithms $A$ and $B$, respectively

Table 2(a), Table 2(c)). The values of the parameters $\Psi_{*j}^{(p)}$, $\Psi_j^{*(p)}$, $\bar{\varphi}_i^{(p)}$, $\underline{\varphi}_i^{(p)}$ $(1 \le p \le \tilde{p})$ in [3] were obtained by the following algorithm: $\tilde{p}$ problems (1), (3), (5), (7)-(9) of modeling the quasiideal stream using the method described, e.g., in [4] with the accuracy parameter $\delta_0 = 25 \cdot 10^{-6}$ (the larger this value, the larger "noise" is simulated in experimental data) for given CC using either Table 1(a) or Table 2(a) or Table 2(c) data (depending on the considered numerical experiment) were solved; parameters $\tau_{*j}^{(p)}$, $\tau_j^{*(p)}$, $\bar{\tau}_i^{(p)}$, $\underline{\tau}_i^{(p)}$ and corresponding stream $\psi_{*j}^{(p)}$, $\psi_j^{*(p)}$ and quasipotential $\bar{\varphi}_i^{(p)}$, $\underline{\varphi}_i^{(p)}$ functions were "memorized"; $\Psi_{*j}^{(p)}$, $\Psi_j^{*(p)}$ were calculated according to the difference representations of formulas $\Psi_*^{(p)}(M) = \frac{\partial \psi_*^{(p)}(M)}{\partial l}, \Psi^{*(p)}(M) = \frac{\partial \psi^{*(p)}(M)}{\partial l}$. It is worth noting that here $\delta_1$ was taken to be orders of magnitude larger than $\delta_0$, since it makes no sense to achieve high accuracy of reconstruction when there are significant errors in the input data [8], [12]. Small values of $\delta_1$ significantly slow down the computational process, which, as evidenced by a number of calculated results, is impractical.

Problems (1), (3), (5), (7)-(9) are solved according to algorithms $A$ and

$B$ for data (13) and with additional conditions corresponding to Table. 1(a), where the parameters of a single burst are identified for different numbers of injections; the results are given in Table 1(b)-Table 1(k). The corresponding etalon and selected reconstructed images are presented in Fig. 2.

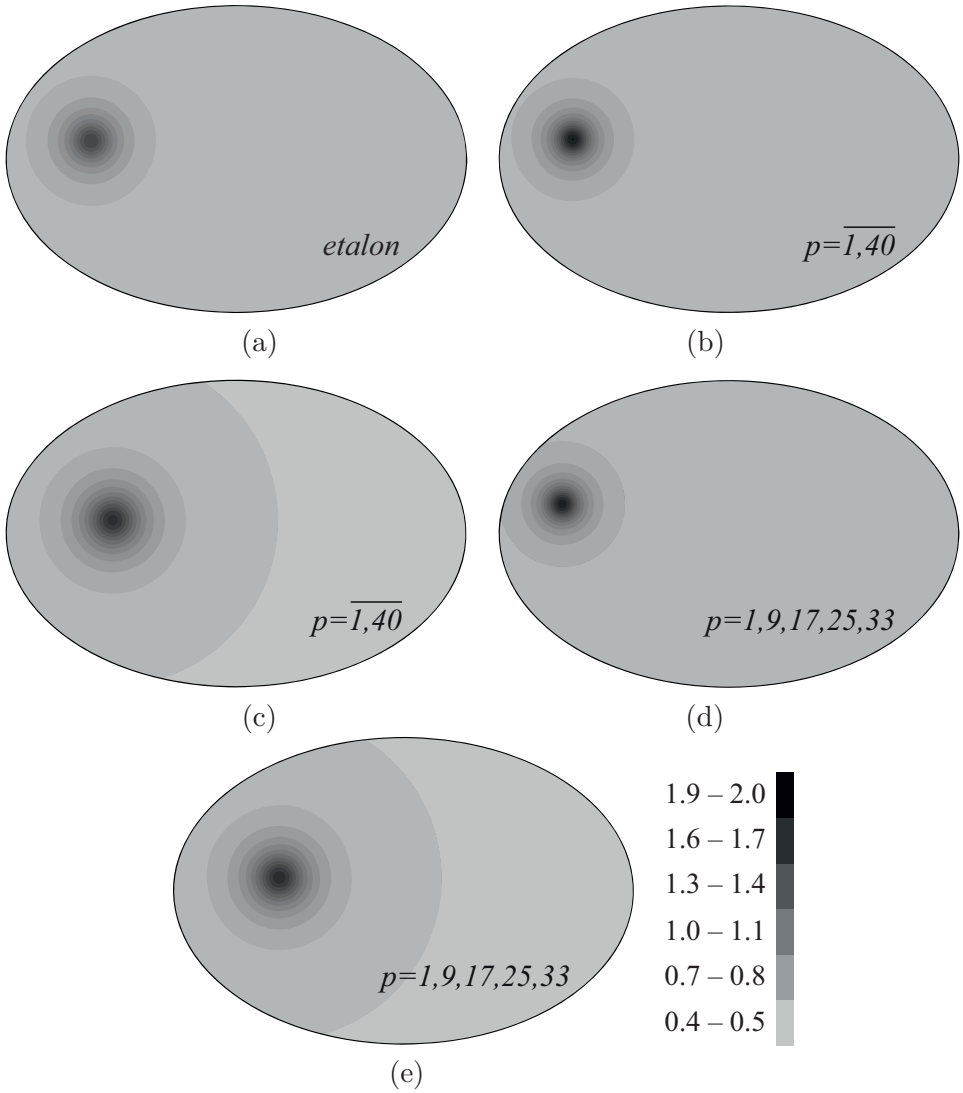


Figure 2: CC distributions for an example with a local burst according to the algorithms $A$ (b, d) and $B$ (c, e) for given etalon (a)

We see that the residuals of coordinates of the reconstructed bursts in com-

parison with the etalon in the case of algorithms $A$ and $B$ for different numbers of injections are as follows: 7.2589 and 14.119, 11.3951 and 14.6686, 15.972 and 14.6428, 61.1756 and 13.6581, 60.3681 and 20.5108, and correspond to Table 1(b)-(f). Considering that impedance tomography methods are most often used for cases of identifying the locations of inhomogeneities [8], [12], algorithm $A$ showed better results than $B$ for $s = 1$ and presence of data from a large number of injections. Moreover, the first of them made it possible to more accurately identify the parameter $\chi$.

Let us now demonstrate the effectiveness of algorithm $A$ for the case of a larger number of bursts. We obtained the results shown in Table 2(b) and Fig. 3(b) under additional conditions in accordance with Table 2(a) (Fig. 3(a)) and (13). In this, the coordinate residuals of the first and second bursts for algorithms $A$ and $B$, respectively, are as follows: 0.7105, 7.8408 (Table 2(b)) and 2.2361, 28.2312 (Table 2(c)). Similarly, in the case of $A$, $\chi$ is better identified. That is, again, algorithm $A$, in comparison with $B$, gives significantly more accurate results.

Comparing the results of algorithms $A$ (Table 2(e)) and $B$ (Table 2(f)) (and corresponding Fig. 3(e) and Fig. 3(f)) under the data (13) and additional conditions previously obtained using Table 2(d), again, the parameters $x_k$, $y_k$ $(k = 1, ..., s)$ are identified more accurately in the first case. The corresponding coordinate residuals of the first, second and third bursts in comparison with the etalon (Table 2(d), Fig. 2(d)) for algorithms $A$ and $B$ are as follows: 21.06, 13.6522, 7.8895 and 15.2643, 19.2354, 7.2111. Similarly, using algorithm $A$, parameter $\chi$ is identified much better.

| | $s$ | $\chi$ | $\alpha_1$ | $\varepsilon_1$ | $x_1$ | $y_1$ | $\alpha_2$ | $\varepsilon_2$ | $x_2$ | $y_2$ | $\alpha_3$ | $\varepsilon_3$ | $x_3$ | $y_3$ |
|---|---|---|---|---|---|---|---|---|---|---|---|---|---|---|
| a) | 2 | 0.5 | 1 | 200 | –95 | –12 | 0.5 | 800 | 0 | 50 | – | – | – | – |
| b) | 2 | 0.5 | 1.3 | 137 | 0 | 58 | 1.4 | 133 | –96 | –12 | – | – | – | – |
| c) | 2 | 0.2 | 0.6 | 10505 | 11 | 24 | 0.8 | 509 | –96 | –10 | – | – | – | – |
| d) | 3 | 0.5 | 1 | 200 | –80 | 30 | 0.5 | 1000 | 50 | 50 | 0.3 | 2000 | 0 | –80 |
| e) | 3 | 0.6 | 1 | 96 | –3 | –73 | 0.9 | 99 | –83 | 51 | 1 | 113 | 48 | 64 |
| f) | 3 | 0.2 | 0.5 | 1852 | –88 | 17 | 0.6 | 8944 | 47 | 31 | 0.3 | 2487 | –6 | –84 |

Table 2: CC distributions for examples with two (a – c) and three (d – f) local bursts, where (a, d) are etalons, (b, e) and (c, f) are calculated according to algorithms $A$ and $B$, respectively

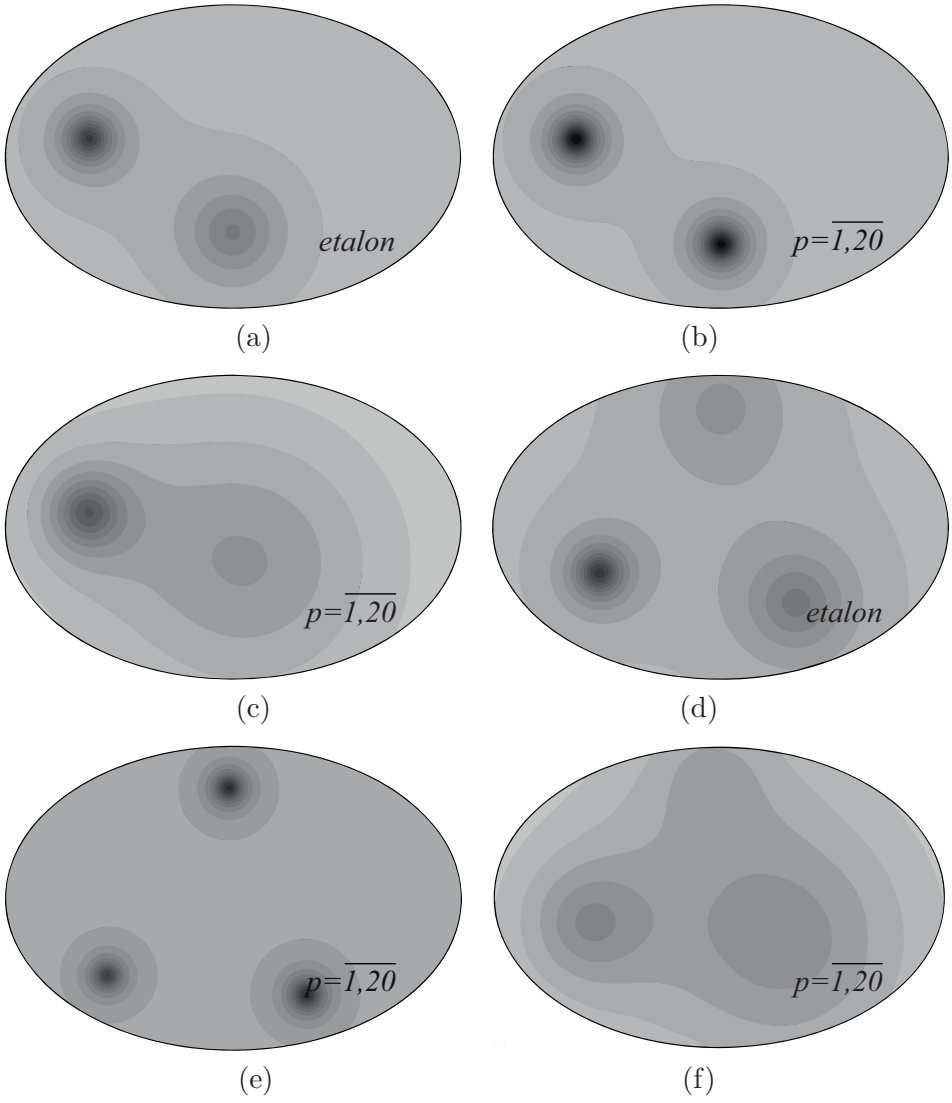


Figure 3: CC distributions for examples with two (a – c) and three (d – f) local bursts according to the algorithms $A$ (b, e) and $B$ (c, f) for given etalons (a, d)

## 5. Conclusion

The complex analysis methodology (method and algorithm) for solving the problems of applied quasipotential tomography developed by us, which assumes

(for each of the respective injections) the presence of only equipotential lines (with the given distributions of local velocities or values of stream functions) and streamlines (with known potential distributions on them) at the domain boundary is modified. This modification involves the application of velocities equality condition using as data the stream and quasipotential functions instead of the procedure of their linearization. The corresponding algorithm involves minimizing the sum of squares of the differences between the calculated and a priori known functions of quasipotential and stream at the boundary of the investigated domain during the alternate parameterization of quasiconformal invariants, internal and boundary nodes of mesh domains $G_z^{\gamma(p)}$, conductivity coefficient using the ideas of the block iteration method. According to the results of numerical calculations of image reconstruction of the environment with existing local bursts, the efficiency of the functional application of the proposed structure is shown in comparison with [3]. Significant advantages of the developed algorithm are the possibility for more accurate identification of coordinates of the sought bursts and their clear separation.

We plan to use both algorithms in combination, taking into account their advantages. Namely: to assess the possibility of extending the functional (10) to space and anisotropy; try to introduce regularization into the algorithm [3]; identify the parameters of piecewise homogeneous and piecewise inhomogeneous anisotropic media, in particular using the functional (10) and conditions of non-ideal contact [10] both inside the object and at sections of quasipotential applications (the latter provides the possibility of implementing a complete electrode model given in [8]).

## References

[1] A. Adler, W.R. Lionheart, Uses and abuses of EIDORS: An extensible software base for EIT, *Physiological Measurement*, **27**, No 5 (2006), S25-S42.

[2] A.Ya. Bomba, M.V. Boichura, *Methods of Complex Analysis in Identification Problems*, National University of Water and Environmental Engineering, Rivne (2020) (in Ukrainian).

[3] A.Ya. Bomba, M.V. Boichura, On a numerical quasiconformal mapping method for the medium parameters identification using applied quasipotential tomography, *Mathematical Modeling and Computing*, **4**, No 1 (2017), 10-20.

[4] A.Ya. Bomba, S.S. Kashtan, D.O. Pryhornytskyi et al., *Complex Analysis Methods*, National University of Water and Environmental Engineering, Rivne (2013) (in Ukrainian).

[5] A.Ya. Bomba, L.L. Kroka, Numerical methods of quasiconformal mappings for solving problems of identifying of electrical conductivity coefficient in an applied potential tomography, *Volyn Mathematical Bulletin. Applied Mathematics series*, **20** (2014), 24-33 (in Ukrainian).

[6] A.Ya. Bomba, M.T. Kuzlo, O.R. Michuta et al., One method of image reconstruction of anisotropic media using applied quasipotential tomographic data, *Mathematical Modeling and Computing*, **6**, No 2 (2019), 211-219.

[7] A.P. Calderon, On an inverse boundary value problem, *Computational and Applied Mathematics*, **25**, No 2-3 (2006), 133-138.

[8] D. Holder, *Electrical Impedance Tomography. Methods, History and Applications*, Institute of Physics, London (2005).

[9] Ja. Malmivuo, R. Plonsey, *Bioelectromagnetism. Principles and Applications of Bioelectric and Biomagnetic Fields*, Oxford University Press, New York (1995).

[10] P.M. Martyniuk, O.R. Michuta, O.V. Ulianchuk-Martyniuk et al., Numerical investigation of pressure head jump values on a thin inclusion in one-dimensional non-linear soil mousture transport problem, *International Journal of Applied Mathematics*, **31**, No 4 (2018), 649-660; DOI: 10.12732/ijam.v31i4.10.

[11] H.A. Oliveira Jr., L. Ingber, A. Petraglia et al., *Stochastic Global Optimization and its Applications with Fuzzy Adaptive Simulated Annealing*, Springer-Verlag, Heidelberg (2012).

[12] Ya.S. Piekkier, K.S. Brazovskii, V.Yu. Usov et al., *Electrical Impedance Tomography*, Scientific and Technical Literature Publishing House, Tomsk (2004) (in Russian).

[13] A.N. Tikhonov, V.Y. Arsenin, *Solution of Ill-posed Problems*, Wiley, New York (1977).